ADVANCED MATERIALS TECHNOLOGIES
www.advmattechnol.de

Inkjet-Printed Soft Resistive Pressure Sensor Patch for Wearable Electronics Applications

*Li-Wei Lo, Hongyang Shi, Haochuan Wan, Zhihao Xu, Xiaobo Tan, and Chuan Wang**

Soft pressure sensors may find a wide range of applications in soft robotics, biomedical devices, and smart wearables. Here, an inkjet-printed resistive pressure sensor that offers high sensitivity and can be fabricated using a very simple process is reported. The device is composed of a conductive silver nanoparticle (AgNP) layer directly printed onto a polydimethylsiloxane substrate and encapsulated by a VHB tape. The pressure is measured through change in electrical resistance caused by pressure-induced strain in the printed AgNP thin film. The influence of substrate stiffness and thickness on the sensitivity and achieved sensors with an optimized configuration that exhibit highly repeatable response with a sensitivity of up to 0.48 kPa^{-1} is systematically studied. It is further demonstrated that such a printed soft sensor patch is capable of measuring arterial pulse waveforms or detecting acoustic vibrations under various sound pressure levels. With its simple and low-cost fabrication process and high sensitivity, the inkjet-printed resistive pressure sensor is promising for future biomedical and smart wearable device applications.

Recent development on smart wearables, health monitoring devices, and soft robotics has attracted a great amount of interest in flexible or stretchable physical and chemical sensors.[1–10] Among the various types of flexible sensors, pressure sensor is one that has been extensively studied, and there is an increasing demand for lightweight, skin-conformable, and disposable soft pressure sensors with high sensitivity.[11–14] There are a number of pressure sensing mechanisms available, including resistive,[15,16] capacitive,[17,18] and piezoelectric.[19,20] Capacitive pressure sensors are typically composed of an elastomeric dielectric layer sandwiched between two parallel-plate electrodes, whose capacitance changes under pressure due to the deformation of the dielectric layer. Although capacitive pressure sensors have some advantages including simple device structure and easy fabrication, they typically exhibit low sensitivity and also require more sophisticated readout circuits that can measure very small capacitance change (typically in the range of hundreds of femtofarad). Moreover, parasitic capacitance and cross-talk between the pixels could also lead to reduced sensitivity and spatial resolution. Piezoelectric materials such as polyvinylidene difluoride that can generate electrical charges from mechanical impact can also be used for pressure sensing.[19] However, such piezoelectric sensors are not suitable for measuring static pressure as they only respond to dynamic changes in pressure. Considering the above, resistive pressure sensors are more promising as they typically offer great sensitivity and only require very basic readout circuit that can measure resistance change. The resistive pressure sensors are typically made using thin films of conductors, such as nanocomposites[15] or nanowires,[16] whose electrical resistance changes under mechanical strain due to microscopic change in morphology or increase in distance between the conductive fillers.[21–23]

For sensor fabrication, inkjet printing[24–33] has been widely used and the advantages are multifold. First, the printing process greatly simplifies the fabrication by completely eliminating the need for masks (used in photolithography), as well as high temperature or high vacuum processes commonly used in semiconductor microfabrication. Moreover, it is an additive and highly scalable process that can greatly reduce materials waste. For these reasons, the inkjet printing process could allow the sensors to be low-cost and potentially disposable. Many types of printed sensors including strain sensor,[29–31] temperature sensor,[24,32] and humidity sensor[27,28] have already been demonstrated.

We have recently demonstrated the use of inkjet-printed silver nanoparticle (AgNP) pattern on an elastomer substrate as an ultrasensitive strain sensor.[31] Inspired by the capability of using printed AgNP thin film for strain sensing and its very high sensitivity, in this work, we demonstrate a printed resistive pressure sensor whose sensing mechanism is based on pressure-induced strain. The sensor consists of a conductive AgNP layer that is directly printed onto a polydimethylsiloxane (PDMS) substrate and subsequently encapsulated by

L.-W. Lo, H. Wan, Z. Xu, Prof. C. Wang
Electrical and Systems Engineering
Washington University in St. Louis
St. Louis, MO 63130, USA
E-mail: chuanwang@wustl.edu
L.-W. Lo, Prof. C. Wang
Institute of Materials Science and Engineering
Washington University in St. Louis
St. Louis, MO 63130, USA
H. Shi, Prof. X. Tan
Electrical and Computer Engineering
Michigan State University
East Lansing, MI 48824, USA
The ORCID identification number(s) for the author(s) of this article can be found under https://doi.org/10.1002/admt.201900717.

DOI: 10.1002/admt.201900717

ADVANCED MATERIALS TECHNOLOGIES
www.advmattechnol.de

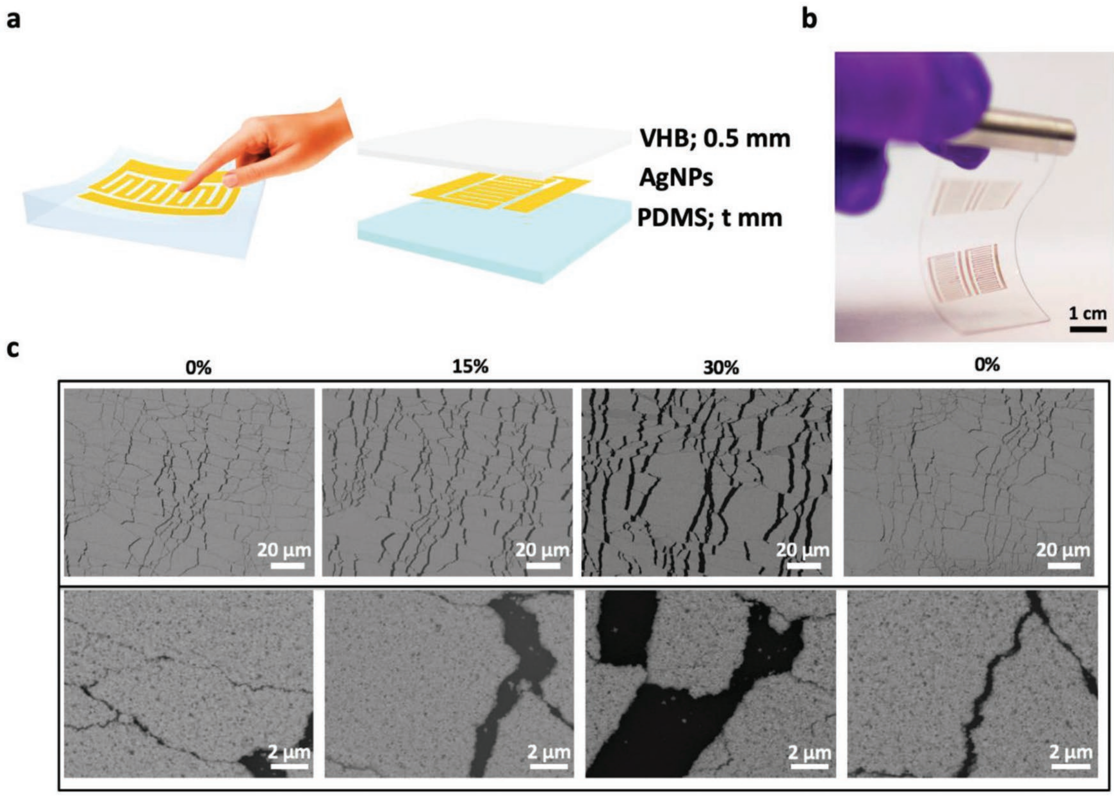

Figure 1. Concept and working principle of the printed resistive pressure sensor. a) Left: schematic illustration of printed resistive pressure sensor. An applied pressure causes deformation in the elastic PDMS substrate, which induces tensile strain in the printed AgNP thin film. Right: Schematic showing the three layers in the pressure sensor. b) Photo of a representative sample with multiple printed pressure sensors. c) SEM images of the printed AgNP thin film under different levels of tensile strain from 0% to 30% and then back to 0% showing the increase in amount and size of microcracks in the film under stretching and the recovery when the strain is released.

a VHB tape. When a pressure is applied perpendicular to the sensor surface, small amount of tensile strain is induced in the AgNP layer, which generates microcracks and leads to a change in electrical resistance. We have systematically studied the influence of substrate stiffness and thickness on the characteristics of the sensor using finite element simulations and achieved an optimized configuration with a pressure sensitivity of up to 0.48 kPa^{-1}. Due to the high sensitivity and low fabrication cost, our printed resistive pressure sensor is particularly suitable for disposable wearable sensor applications. As proof-of-concept, we have demonstrated the use of the printed sensor for detecting acoustic vibration and measuring arterial pulse waveforms.

The concept and structure of the printed resistive pressure sensor are schematically illustrated in **Figure 1**a. The device is composed of three layers: the elastic PDMS substrate, printed AgNP thin film, and VHB tape encapsulation. The thickness of the VHB tape is 0.5 mm, while the thickness of the PDMS substrate varies from 1 to 0.15 mm. As will be discussed later, both the thickness and stiffness of the PDMS have great impact on the sensitivity of the sensor. Due to the hydrophobicity of PDMS, pretreating the PDMS substrate with oxygen plasms prior to printing is crucial as it greatly improves the wetting of the ink on the surface and consequently the uniformity of the printed AgNP thin film. As shown in Figure 1a, the active sensing region of the device is comprised of a serpentine-shaped printed AgNP pattern, and the whole device is encapsulated by a VHB tape which is stretchable and also offers strong bonding to low surface energy surfaces, such as PDMS. More details of the sensor fabrication process are described in the Experimental Section and the printed device geometry is presented in Figure S1 (Supporting Information). The printing process allows the sensors to be easily fabricated in large quantity and at low cost. A photograph of a roll of PDMS substrate with multiple printed sensors is shown in Figure 1b.

The sensing mechanism of the printed resistive pressure sensor can be attributed to the formation of microcracks inside the AgNP thin film under pressure. As illustrated in the left schematic in Figure 1a, pressure applied perpendicular to the surface of the sensor causes deformation of the substrate, which induces a tensile strain in the printed AgNP thin film and leads to the formation of microcracks. The microcracks will result in an increase in the film resistance and the change can be measured electrically. In order to understand the relation between the microcracks and tensile strain, a PDMS substrate with printed AgNP thin film was mounted on a linear stretching stage and examined by scanning electron microscope (SEM). Figure 1c shows the SEM images taken from the printed AgNP thin film when the sample was stretched under various levels of tensile strain from 0%, 15% to 30% then released to its relaxed state of 0%. The AgNPs are 100–200 nm in diameter (as shown in Figure S2, Supporting Information) and they are

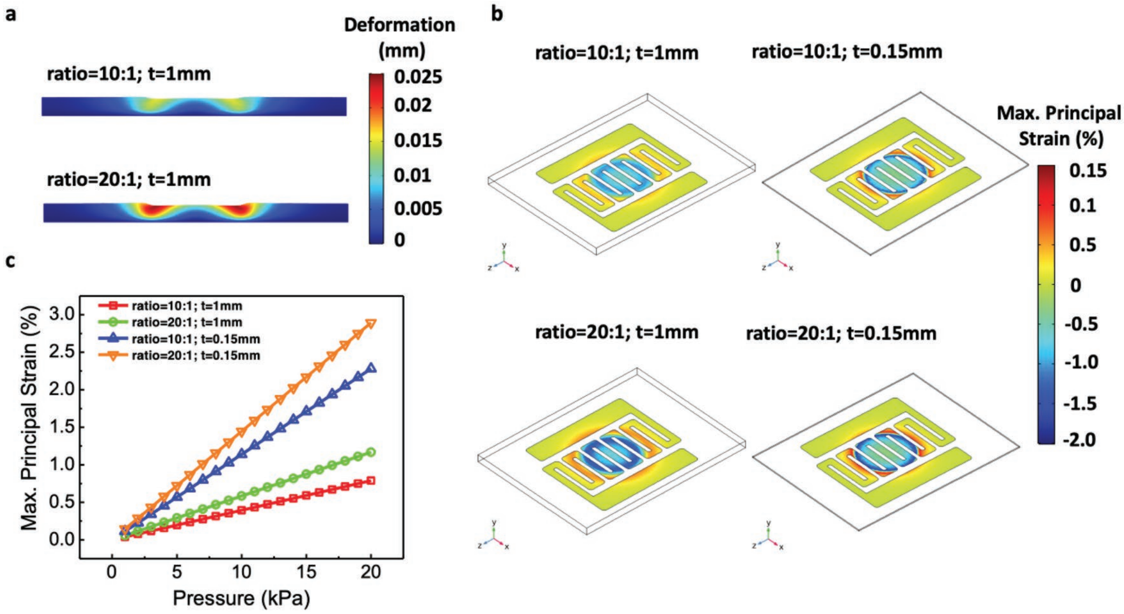

Figure 2. Finite element simulation showing the pressure-induced deformation and strain in four types of sensors with different PDMS mixing ratio (10:1 and 20:1) and substrate thickness (1 and 0.15 mm). a) Deformation in two 1 mm thick sensors with mixing ratio of 10:1 and 20:1 when a pressure of 10 kPa was applied. b) Profile of the maximum principal strain in four types of sensors when a pressure of 10 kPa was applied perpendicular to the sensor surface. c) Maximum principal strain plotted as a function of pressure for four types of sensors.

mostly bonded together in relaxed state. From both low magnification (top row) and high magnification (bottom row) images, one can clearly see that an increase in strain leads to increase in both the amount and size of the microcracks and such microcracks propagate uniformly through the entire printed AgNP pattern. On the other hand, when the strain is released, the size of the microcracks becomes smaller and the film morphology is recovered to almost the same as the relaxed state. The crack formation and recovery processes are reversible, and it is the reason for the highly repeatable electrical response from the sensor.

Because the response of the sensor depends on the strain induced by the substrate deformation, it is important to understand the effect of substrate stiffness and thickness on the induced strain. Finite element simulations were conducted using COMSOL to investigate four different types of sensors with different PDMS stiffness and thickness and the results are presented in **Figure 2**. The variation in PDMS stiffness was achieved by mixing PDMS prepolymer and curing agent at a mixing ratio of either 10:1 (stiffer) or 20:1 (softer), and two different PDMS substrate thicknesses of either 1 or 0.15 mm were prepared. Figure 2a displays the simulated deformation under 10 kPa pressure in two samples with 1 mm thick PDMS and mixing ratios of 10:1 or 20:1. The PDMS with a 20:1 mixing ratio results in a softer substrate with a Young's modulus of 2.8×10^5 Pa and the 10:1 mixing ratio results in a stiffer substrate with a Young's modulus of 5.8×10^5 Pa.[34] Simulation results show the softer sample with 20:1 mixing ratio deforms significantly more than the stiffer 10:1 sample. The larger deformation will translate to higher sensitivity as will be discussed later. Furthermore, we have also simulated the maximum principal strain profile for each sample and the results are presented in Figure 2b. By comparing the results, one can see that under the same pressure, the samples with thinner (0.15 mm) or softer (20:1) substrate experience greater maximum principal strain compared to the samples with thicker (1 mm) or stiffer (10:1) substrates, respectively. The simulation results also indicate that the greater the substrate deformation, the larger the maximum principal strain induced. Figure 2c summarizes the simulation results of maximum principal strain in all four types of sensors under various pressure levels up to 20 kPa. The results indicate that the maximum strain varies linearly with the applied pressure, and among all samples, the one with a PDMS thickness of 0.15 mm and 20:1 mixing ratio exhibits the largest maximum principal strain under all the conditions.

From the simulation results above, one can expect that the printed sensors with thinner and softer substrate will have more and larger microcracks formed under the same pressure level, which will result in greater change in electrical resistance and better sensitivity. To understand and experimentally test the relation between the pressure/strain and the electrical properties of the printed AgNP thin film, the relative changes in resistance of the sensor ($\Delta R/R_0$, where ΔR is the change in resistance and R_0 is the resistance in relaxed state) were measured as a function of pressure or tensile strain and the results are presented in **Figure 3**. The details about the electromechanical property measurement setup are described in the Experimental Section and the pressure applied onto the printed sensor was precisely determined using a commercially available force sensor as a reference. Figure 3a shows the sensor response curve ($\Delta R/R_0$ vs P) for all four types of printed sensors described in Figure 2. All of them responded similar to the applied pressure and exhibited a linear relationship with increasing pressure from 0 to about 15 kPa. The sensitivity of the sensor can be extracted from the slope of the $\Delta R/R_0$ vs P curve and the results are plotted in Figure 3b. The sample

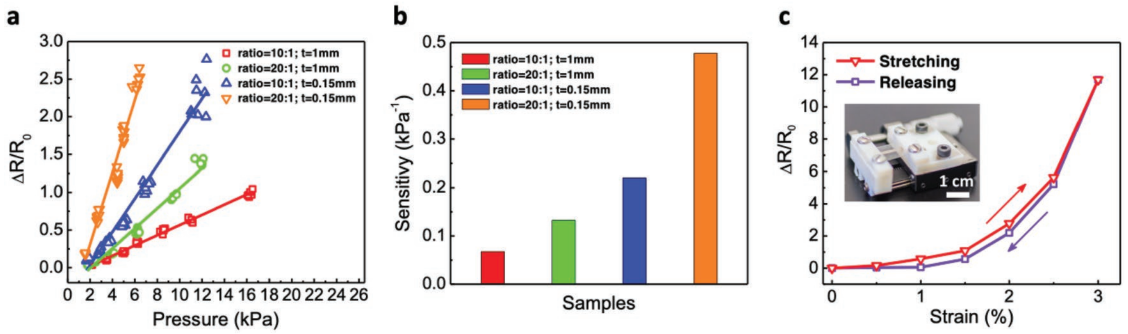

Figure 3. Electromechanical characterization of the printed resistive pressure sensor. a) Relative change in resistance in response to applied pressure for four types of sensors. b) The sensitivity of each type of sensor extracted from the data in panel (a). c) Relative change in resistance plotted as a function of tensile strain, where the printed AgNP thin film is manually stretched and released by a linear stretching stage.

with the softest and thinnest PDMS substrate (20:1 mixing ratio and 0.15 mm thickness) exhibits the highest sensitivity of 0.48 kPa^{-1}. The rest of the samples with mixing ratio of 10:1 and thickness of 0.15 mm, mixing ratio of 20:1 and thickness of 1 mm, and mixing ratio of 10:1 and thickness of 1 mm all exhibit lower sensitivity of 0.22, 0.13, and 0.07 kPa^{-1}, respectively. The experimental results again indicate that better sensitivity can be achieved by using thinner and softer PDMS substrate, which is in good agreement with the simulation results above in Figure 2c. Furthermore, the sensitivity of 0.48 kPa^{-1} is higher than widely reported capacitive pressure sensors, whose sensitivity typically range from as low as ≈0.002[18] to 0.15 kPa^{-1} with texturized dielectric layer prepared using sophisticated microfabrication process.[35] The sensitivity is also comparable with many previously reported resistive pressure sensors based on various types of sensing materials (Table S1, Supporting Information). In addition, unlike most pressure sensors that exhibit nonlinear response to pressure with the highest sensitivity happening at low pressure range, our printed pressure sensor exhibits a linear pressure response curve throughout its detecting range.

In order to confirm that the observed resistance change under pressure is indeed caused by pressure-induced tensile strain, a straight line of AgNP was printed onto PDMS and the sample was mounted on a linear stage for stretching test as shown in Figure 3c. The sample was first stretched from 0% to 3% and an increase in $\Delta R/R_0$ of up to 12 (1200%) was observed. Then the sample was gradually released to its relaxed state and the $\Delta R/R_0$ fully recovered to around 0 with almost hysteresis-free resistance-strain characteristic. The stretching test result links the experiment results in Figure 3a to the simulation results in Figure 2c and explains the working principle of the printed resistive pressure sensor—pressure induces strain, which leads to formation of microcracks in the printed AgNP thin film and consequently increase in its electrical resistance.

The dynamic response and stability of the printed resistive pressure sensor were also studied and the results are presented in **Figure 4**a,b. The pressure was applied automatically using a modified syringe pump shown in Figure 4c. Various pressure levels can be applied by controlling the infuse rate, withdraw rate, and target volume in the syringe pump. In this setup, the printed sensor was placed on top of a commercially available

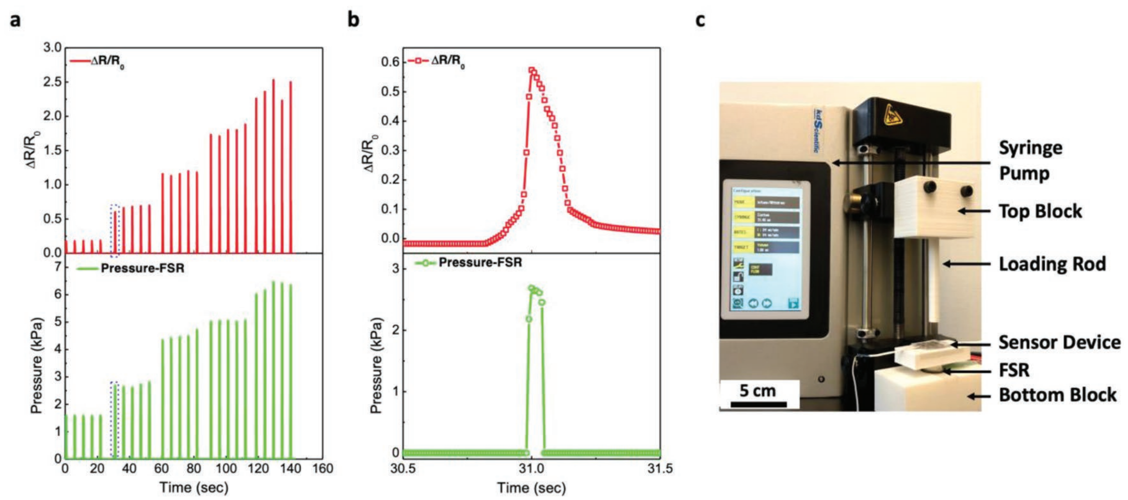

Figure 4. Dynamic response test of the sensor under different pressure. a,b) Plots showing the relative changes in resistance for the pressure sensor with 20:1 mixing ratio and 0.15 mm thickness under dynamic pressure test in a range from 1.5 to 6.5 kPa at a frequency of 0.2 Hz. The red trace shows the resistance change of the sensor and the green trace corresponds to the applied pressure. The data in (b) are a zoomed-in view of the data inside the blue dashed box in panel (a). c) Photograph showing the experimental setup used for testing the dynamic response of the sensor.

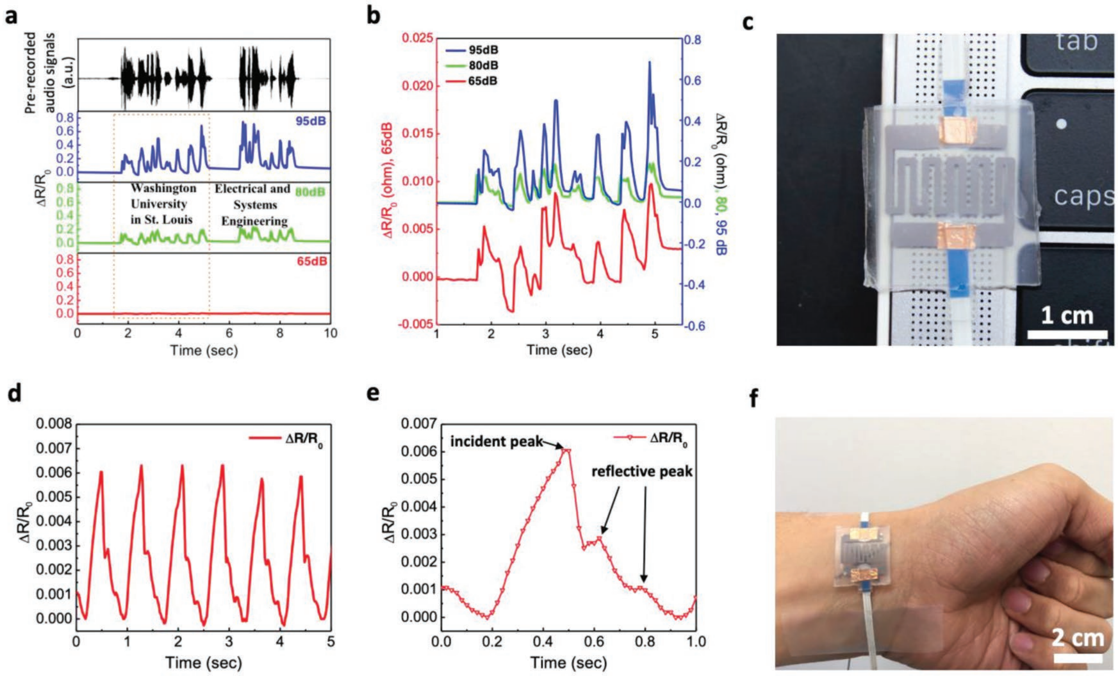

Figure 5. Representative applications of the printed resistive pressure sensor. a,b) Relative change in resistance of the printed pressure sensor in response to acoustic vibrations under various sound pressure levels (SPL) played through a speaker with prerecorded voice (Washington University in St. louis, Electrical and System Engineering). c) Photograph showing the experiment setup with the sensor placed directly on a laptop speaker. d) Arterial pulse waveforms measured from the printed sensor. e) One cycle of the data in (d) showing the incident peak and reflective peak of the arterial pulse waveform. f) Photograph of the printed pressure sensor attached on the wrist above the artery for the experiment.

force sensor (FSR 402 Interlink Electronics, Inc.) which precisely measures the pressure applied by the loading rod. The device with the best sensitivity (20:1 mixing ratio and 0.15 mm thickness) was used for the dynamic response measurement. Pressure was applied at a frequency of 0.2 Hz and repeated for five times at each pressure level from ≈1.5 to 6.5 kPa and the corresponding resistance of the sensor was recorded as a function of time. As shown in Figure 4a, the $\Delta R/R_0$ exhibits highly reproducible sensing response of about 0.24, 0.6, 1.2, 1.6, and 2.25 at pressure levels of 1.5, 2.8, 4.5, 5.1, and 6.5 kPa, respectively. Figure 4b plots one cycle of the dynamic response data, from which the response and recovery times are estimated to be both at around 0.25 s. It is worth noting that our printed sensor exhibits slightly slower response than the commercial force sensor, which is due to the slow recovery characteristics of the PDMS substrate. Except for the longer response time, the data measured from our printed pressure sensor (red trace) closely tracks the data from the reference force sensor indicating the reliability of our device for practical applications. We have also tested the cyclic durability of the sensor by repeatedly applying a pressure of 1.5 kPa at a frequency of 0.1 Hz for up to 1000 cycles and long-term stability of the sensor by measuring the response curve of same device after 5 months. In both cases, the sensor response remained almost unchanged and the data are presented in Figures S3 and S4 (Supporting Information).

Due to its stretchability, small thickness, and the extremely high pressure sensitivity, our printed resistive pressure sensor is suitable for a wide range of applications such as wearable health monitoring device or sensory system for soft robots. As a proof of concept, we demonstrate two different applications using the printed sensor—a soft microphone patch (**Figure 5**a,c) and a wearable patch for arterial pulse monitoring (Figure 5d,f). For the microphone application, a sensor (20:1, 0.15 mm thickness) was placed on a laptop speaker as shown in Figure 5c. A prerecorded audio file of a person speaking "Washington University in St. Louis, Electrical and Systems Engineering" was played though the speaker at three different volume settings, corresponding to sound pressure levels (SPL) of 95, 80, and 65 dB, respectively. The acoustic response from the sensor ($\Delta R/R_0$) was recorded and plotted in Figure 5a. Notably, as the volume increases, the magnitude of the response recorded by the sensor also increases, but the signal waveform remains almost identical as indicated in Figure 5b. The signal measured from the printed sensor also closely resembles the waveform from the source file, albeit the sampling rate was much lower at 20 Hz (compared to 44.1 kHz of the source file), which is limited by the step size of 50 ms from the Semiconductor Device Analyzer used during the measurements. The demonstration above indicates the potential of our printed sensor for wearable audio recording device or sounds recognition applications.

Moreover, the high sensitivity and stretchability of the sensor make it also suitable for application as a wearable health monitoring device. The stretchability ensures its ability to conformably attach to human skin and its extremely high sensitivity enables it to record weak signals from the body. Here, we demonstrate that our printed sensor can be used as a noninvasive, real-time arterial pulse measurement patch as shown in Figure 5d,c. In order to record the arterial pulse waveform accurately, the sensor was placed on top of the wrist artery as shown in Figure 5f and a wrist band was used to tightly wrap the sensor around the wrist. The recorded pulse waveform shown in Figure 5d is periodic and corresponds to a heart rate of 81 bpm. The peripheral artery pressure waves include three waves, the incident wave generated from the ejection of the blood from the heart, the reflected waveform from the upper body region and the reflected wave from the lower body. In Figure 5e, the waveform clearly shows the incident peak (P_1) and two reflected peaks (P_2 and P_3). From these peaks, one can determine the arterial stiffness by radial artery augmentation index $AI_r = P_2/P_1$, and the time difference between the first two peaks, ΔT_{vap}. The measured value from a 25-year-old test person shows $AI_r \approx 0.45$ and $\Delta T_{vap} \approx 0.16$, both of which are expected values according to the literature.[36] The ability to accurately measure the arterial pulse waveform makes it possible to further implement our sensor into a real-time blood pressure monitoring device in the future.

In summary, we have demonstrated a printed resistive pressure sensor that is easy to fabricate, soft, lightweight, and with high sensitivity. The sensing mechanism of the sensor including pressure-induced strain, microcrack formation, and effect of substrate stiffness and thickness on the sensor performance has been systematically studied by both simulation and experiments. Due to its high sensitivity, the pressure sensor is able to measure both sound wave and arterial pulse waveform. The sensor platform developed in this work may lead to disposable sensor patches that can be used in future smart wearables and biomedical devices for applications such as real-time blood pressure monitoring.

Experimental Section

Sensor Fabrication: To prepare the substrate, PDMS prepolymer was first mixed with the curing agent (Sylgard 184, Dow Corning, USA) with mixing ratios of either 10:1 or 20:1 w/w. The PDMS was then casted onto a 1 in. × 1 in. glass slide pretreated with Rain-X (ITW Global Brands) and isopropanol. The 1 mm thick substrate was prepared by sandwiching the PDMS in between two glass slides with a 1 mm spacer and the 0.15 mm thick substrate was prepared by spin coating (500 rpm, 30 s). The PDMS substrate was then cured on a hotplate for 3 h at 80 °C. Silver nanoparticle ink (PG-007AA from Paru Corporation, South Korea) with particle size of 100–200 nm was diluted in ethylene glycol and then printed onto the PDMS substrate using a GIX Microplotter (Sonoplot Inc.) with nozzle openings of 50–200 µm. To aid the wetting of the ink, the PDMS substrate was treated by oxygen plasma (Plasma Etch PE25, Plasma Etch Inc.) at 30 W for 5 s. After printing the AgNP feature, the sample was placed on a hotplate and annealed for 20 min at 55 °C to remove the polymer binders and then for another 60 min at 150 °C remove the solvent and sinter the silver nanoparticles. As a last step, flexible ribbon cables were used to form electrical connection with the printed sensor and the entire device was packaged by VHB tape (VHB-4905, 3M) to serve as an encapsulation layer. The VHB tape made with acrylic foam is viscoelastic which is desirable for stretchable sensor applications and it also bonds strongly with the low surface energy PDMS substrate.

Pressure Measurement: A modified syringe pump with 3D-printed loading rod and loading platform was used for the pressure measurement. A commercially available force sensor (FSR 402, Interlink Electronics, Inc.) was attached to the bottom of the loading platform as a reference sensor to measure the actual pressure exerted by the loading rod. During the experiment, the pressure was applied to both the printed AgNP sensor and the FSR reference sensor and the data from both sensors were record by a Semiconductor Device Analyzer (Keysight B1500A). Before placing the AgNP sensor, the response curve (resistance-pressure) of the FSR sensor was characterized by placing different amount of standard weight on the loading platform.

Device Characterization: Both optical microscope (Olympus BX53M) and field-emission scanning electron microscope (JEOL JSM-7001LVF) were used to capture the surface morphology of the printed AgNP thin film. Semiconductor Device Analyzer (Keysight B1500A) was used to measure the electrical properties of AgNP sensor. For each measurement, a constant voltage of 1 V was applied the current through the sensor was measured by the analyzer, from which the resistance value was deduced. The experiment involving human subject has been performed with the full, informed consent of the volunteer, who is also the first author of the manuscript.

Supporting Information

Supporting Information is available from the Wiley Online Library or from the author.

Acknowledgements

This work was partially funded by a Washington University Collaboration Initiation Grant (CIG) and a Michigan State University Foundation Strategic Partnership Grant (No. 16-SPG-Full-3236). The authors acknowledge the financial support from Washington University in St. Louis and the Institute of Materials Science and Engineering for the use of instruments and staff assistance.

Conflict of Interest

The authors declare no conflict of interest.

Keywords

printed electronics, resistive pressure sensors, stretchable electronics, wearable devices

Received: August 21, 2019
Revised: October 18, 2019
Published online: November 13, 2019

[1] Y. Yamamoto, D. Yamamoto, M. Takada, H. Naito, T. Arie, S. Akita, K. Takei, *Adv. Healthcare Mater.* **2017**, *6*, 1700495.
[2] W. Honda, S. Harada, T. Arie, S. Akita, K. Takei, *Adv. Funct. Mater.* **2014**, *24*, 3299.
[3] W. Gao, S. Emaminejad, H. Y. Y. Nyein, S. Challa, K. Chen, A. Peck, H. M. Fahad, H. Ota, H. Shiraki, D. Kiriya, D. H. Lien, G. A. Brooks, R. W. Davis, A. Javey, *Nature* **2016**, *529*, 509.
[4] X. Huang, Y. Liu, K. Chen, W. J. Shin, C. J. Lu, G. W. Kong, D. Patnaik, S. H. Lee, J. F. Cortes, J. A. Rogers, *Small* **2014**, *10*, 3083.
[5] I. You, B. Kim, J. Park, K. Koh, S. Shin, S. Jung, U. Jeong, *Adv. Mater.* **2016**, *28*, 6359.
[6] G. Schwartz, B. C. K. Tee, J. Mei, A. L. Appleton, D. H. Kim, H. Wang, Z. Bao, *Nat. Commun.* **2013**, *4*, 1859.
[7] S. Nakata, T. Arie, S. Akita, K. Takei, *ACS Sens.* **2017**, *2*, 443.
[8] S. Harada, W. Honda, T. Arie, S. Akita, K. Takei, *ACS Nano* **2014**, *8*, 3921.

[9] C. Wang, D. Hwang, Z. Yu, K. Takei, J. Park, T. Chen, B. Ma, A. Javey, *Nat. Mater.* **2013**, *12*, 899.
[10] Y. Cao, J. Figueroa, W. Li, Z. Chen, Z. Lin Wang, N. Sepúlveda, *Nano Energy* **2019**, *63*, 103852.
[11] M. Gao, L. Li, Y. Song, *J. Mater. Chem. C* **2017**, *5*, 2971.
[12] Q. Huang, Y. Zhu, *Adv. Mater. Technol.* **2019**, *4*, 1800546.
[13] N. N. Jason, M. D. Ho, W. Cheng, *J. Mater. Chem. C* **2017**, *5*, 5845.
[14] B. Zhu, Y. Ling, L. W. Yap, M. Yang, F. Lin, S. Gong, Y. Wang, T. An, Y. Zhao, W. Cheng, *ACS Appl. Mater. Interfaces* **2019**, *11*, 29014.
[15] S. Y. Kim, H. Lim, J. Hong, H. Ko, J. Park, Y. Lee, Y.-D. Jung, M. Ha, *ACS Nano* **2014**, *8*, 4689.
[16] S. Gong, W. Schwalb, Y. Wang, Y. Chen, Y. Tang, J. Si, B. Shirinzadeh, W. Cheng, *Nat. Commun.* **2014**, *5*, 3132.
[17] S. Park, H. Kim, M. Vosgueritchian, S. Cheon, H. Kim, J. H. Koo, T. R. Kim, S. Lee, G. Schwartz, H. Chang, Z. Bao, *Adv. Mater.* **2014**, *26*, 7324.
[18] H. Shi, M. Al-Rubaiai, C. M. Holbrook, J. Miao, T. Pinto, C. Wang, X. Tan, *Adv. Funct. Mater.* **2019**, *29*, 1809116.
[19] S. H. Park, H. B. Lee, S. M. Yeon, J. Park, N. K. Lee, *ACS Appl. Mater. Interfaces* **2016**, *8*, 24773.
[20] E. J. Curry, K. Ke, M. T. Chorsi, K. S. Wrobel, A. N. Miller, A. Patel, I. Kim, J. Feng, L. Yue, Q. Wu, C.-L. Kuo, K. W.-H. Lo, C. T. Laurencin, H. Ilies, P. K. Purohit, T. D. Nguyen, *Proc. Natl. Acad. Sci. USA* **2018**, *115*, 909.
[21] D. Kang, P. V. Pikhitsa, Y. W. Choi, C. Lee, S. S. Shin, L. Piao, B. Park, K. Y. Suh, T. Il Kim, M. Choi, *Nature* **2014**, *516*, 222.
[22] Y. W. Choi, D. Kang, P. V Pikhitsa, T. Lee, S. M. Kim, G. Lee, D. Tahk, M. Choi, *Sci. Rep.* **2017**, *7*, 40116.
[23] T. Yang, W. Wang, H. Zhang, X. Li, J. Shi, Y. He, Q.-S. Zheng, Z. Li, H. Zhu, *ACS Nano* **2015**, *9*, 10867.
[24] D. Kong, L. T. Le, Y. Li, J. L. Zunino, W. Lee, *Langmuir* **2012**, *28*, 13467.
[25] L. Cai, S. Zhang, J. Miao, Z. Yu, C. Wang, *ACS Nano* **2016**, *10*, 11459.
[26] L. Cai, S. Zhang, Y. Zhang, J. Li, J. Miao, Q. Wang, Z. Yu, C. Wang, *Adv. Mater. Technol.* **2018**, *3*, 1700232.
[27] H. Andersson, A. Manuilskiy, T. Unander, C. Lidenmark, S. Forsberg, H.-E. Nilsson, *IEEE Sens. J.* **2012**, *12*, 1901.
[28] F. Molina-Lopez, D. Briand, N. F. De Rooij, *Sens. Actuators, B* **2012**, *166–167*, 212.
[29] B. Ando, S. Baglio, *IEEE Sens. J.* **2013**, *13*, 4874.
[30] F. Michelis, L. Bodelot, Y. Bonnassieux, B. Lebental, *Carbon* **2015**, *95*, 1020.
[31] S. Zhang, L. Cai, W. Li, J. Miao, T. Wang, J. Yeom, N. Sepúlveda, C. Wang, *Adv. Electron. Mater.* **2017**, *3*, 1700067.
[32] T. Vuorinen, J. Niittynen, T. Kankkunen, T. M. Kraft, M. Mäntysalo, *Sci. Rep.* **2016**, *6*, 35289.
[33] J. Jiang, B. Bao, M. Li, J. Sun, C. Zhang, Y. Li, F. Li, X. Yao, Y. Song, *Adv. Mater.* **2016**, *28*, 1420.
[34] J. Y. Park, S. J. Yoo, E. J. Lee, D. H. Lee, J. Y. Kim, S. H. Lee, *BioChip J.* **2010**, *4*, 230.
[35] S. C. B. Mannsfeld, B. C. K. Tee, R. M. Stoltenberg, C. V. H. H. Chen, S. Barman, B. V. O. Muir, A. N. Sokolov, C. Reese, Z. Bao, *Nat. Mater.* **2010**, *9*, 859.
[36] W. W. Nichols, *Am. J. Hypertens.* **2005**, *18*, 3.